Energy dependence of the $^{12}C(p,\pi^+)^{13}C^*$ reaction in the region of the Δ_{1232} resonance

G. M. Huber, G. J. Lolos, E. L. Mathie, and Z. Papandreou
Department of Physics and Astronomy, University of Regina, Regina, Saskatchewan, Canada S4S 0A2

K. H. Hicks, P. L. Walden, and S. Yen
TRIUMF, Vancouver, British Columbia, Canada V6T 2A3

X. Aslanoglou
Department of Physics, Florida State University, Tallahassee, Florida 32306

E. G. Auld
Department of Physics, University of British Columbia, Vancouver, British Columbia, Canada V6T 2A6

W. R. Falk
Department of Physics, University of Manitoba, Winnipeg, Manitoba, Canada R3T 2N2
(Received 23 March 1987)

Differential cross sections for the $^{12}C(p,\pi^+)^{13}C^*$ reaction at $T_p=250$, 354, and 489 MeV are presented and compared with previously published data taken at other energies in the Δ_{1232} resonance region. At fixed four momentum transfers greater than 0.4 GeV^2/c^2, the differential cross sections exhibit a maximum near the invariant mass of the Δ_{1232}. This energy dependence is similar to that shown by the $pp\rightarrow d\pi^+$ reaction at equivalent energy, and provides strong evidence of a $NN\rightarrow NN\pi^+$ process in the (p,π^+) reaction mechanism. The total cross section for each transition exhibits a maximum at an energy about 100 MeV lower than that expected from the Δ_{1232} invariant mass. This energy dependence could be the result of an interplay between the increase in cross section due to the role of the Δ_{1232} in the (p,π^+) reaction mechanism, and the decrease in cross section due to the large momentum transfers that the reaction is restricted to at higher energies.

INTRODUCTION

For approximately the last 15 years since the first (p,π^+) angular distributions were obtained at Uppsala,[1] there has been a sustained interest in (p,π) reactions.[2–5] This is largely because exclusive (p,π) reactions are characterized by a large value of momentum transferred to the struck nucleus compared to the nuclear Fermi momentum, or compared to the momentum transferred by most other nuclear reactions. Thus, it was originally hoped that (p,π) reactions would be a useful spectroscopic tool for studying the high momentum components of nuclear wave functions provided that the reaction mechanism was well understood. Unfortunately, this lack of understanding of the reaction mechanism has proved to be a major stumbling block, and the original interest has now shifted to the problem of trying to understand the basic pion production mechanism within the nuclear environment.

Experimentally, most of the work on targets heavier than ^{3}He has been near the pion production threshold, in the region 150–250 MeV, although there have been a limited number of measurements at higher energies, primarily in the region above 600 MeV.[4] On ^{12}C, which is experimentally one of the most studied targets, there is a gap between 250 and 800 MeV in which the only angular distribution that has been obtained was for the $^{12}C(p,\pi^+)^{13}C_{g.s.}$ reaction via the time reversed (π^+,p) reaction at an equivalent proton energy of 332 MeV.[6] Thus, there is a large dynamic range in which very little is known about the $^{12}C(p,\pi^+)^{13}C^*$ reaction.

This region is important because in it the (p,π^+) reaction is expected to show the effects of a Δ_{1232} excitation via the $NN\rightarrow NN\pi^+$ process. A simple calculation shows that the peak of the Δ_{1232} excitation would occur at a beam energy of 321 MeV if the beam proton and ^{12}C target combined to form a mass-13 nucleus with one nucleon excited to a mass of 1232 MeV. A similar calculation for the $pp\rightarrow d\pi^+$ reaction would predict a peak cross section due to the Δ_{1232} at a beam energy of 634 MeV, as has been well noted.[7] A maximum in the differential cross section near 321 MeV has indeed already been noted on ^{10}B at several different fixed momentum transfers.[8] However, the energy dependence of the total cross section has never before been measured. It is hoped that angular distribution measurements in this region will aid in the understanding of the basic (p,π^+) reaction mechanism.

THE EXPERIMENT

The experiment was performed with the Medium Resolution Spectrometer (MRS) at TRIUMF during two runs using an unpolarized proton beam whose intensity

was in the range of 5–25 nA. The beam was incident on a research grade natural carbon target of 92 mg/cm^2 thickness. The systematic error corresponding to nonuniformities in this target thickness and errors in the measurement of this thickness is estimated to be less than 1%. The target angle with respect to the beam was chosen so that the energy loss of the proton beam and the energy loss of the detected pions would be approximately equal. An error of 2° in the target angle calibration corresponds to a relative uncertainty in the target thickness of 4%.

Beam intensity was monitored continuously by an in-beam polarimeter and by a secondary emission monitor (SEM), both of which were previously calibrated against a Faraday cup. The polarimeter consisted of a CH_2 target of 1.383 mg/cm^2 thickness and two pairs of counter telescopes, each in coincidence with a recoil counter, that count elastic proton-proton scattering events. When both monitors worked properly, agreement between the two monitors for total charge on target was about 2%. In cases when the two monitors disagreed by more than this amount, the SEM was used since the thin polarimeter target has been known to warp after an extended time period in the beam. The location and size of the beamspot (typically 2.5 cm$\times$0.5 cm XY in dispersed mode) was visually monitored periodically with a scintillator located at the target position.

Because the CAMAC scalers of the MRS are not inhibited when the data acquisition system is busy, all scalers must be corrected by the live time of the instrument. This live time was measured by two independent means. The live time can be simply measured by taking the ratio of the number of busy latches that the data acquisition electronics generates divided by the number of event triggers. The MRS electronics also contains a provision for generating pseudo-events electronically; the ratio of the number of these pseudo-events actually seen by the acquisition system, divided by the number of pseudo-events generated, gives a second determination of the live time. In most cases the two different methods were within 3% of each other; the live time varied between 60% and 95%, depending on the event rate.

The spectrometer acceptance was calibrated at 500 MeV using the $pp \rightarrow d\pi^+$ reaction, whose cross section is known to a high precision;[9] the proton energy was chosen so that pions from this reaction would have approximately the same momentum as pions from the $^{12}C(p,\pi^+)^{13}C$ reaction at 354 MeV. The effective solid angle of the spectrometer, determined by this method, was 2.1 msr, with a standard deviation of 0.1 msr between independent calibrations. This solid angle was found to be independent of beamspot size and pion energy within this uncertainty.

The spectrometer detection system consisted of a multiwire drift chamber located in front of the spectrometer's entrance quadrupole magnet, and two vertical drift chambers followed by two planes of plastic scintillators located near the focal plane of the spectrometer. The two planes of scintillators, along with one plane of the front end chamber, and one plane of the first of the two vertical drift chambers, provided the event definition. This arrangement still permitted enough information to be written on tape so that the efficiency of each drift chamber could be determined from the experimental data. The product of the efficiency of all three chambers was typically 75%, although at extreme backangles the product fell as low as 35%. This decrease in efficiency was shared equally between all three chambers, and was primarily due to increased beam current at back angles in order to reduce the running time, resulting in increased singles rates from background.

The use of a front end wire chamber provides a high degree of redundancy as it allows a complete ray trace through the spectrometer back to the target, a distance of about 11 m; therefore, all background sources not originating from the illuminated target spot could be eliminated. Most of the muons resulting from pion decay within the spectrometer were eliminated via the beam spot and solid angle cuts; net events observed were then corrected for pion decay within the spectrometer. At 250 MeV the pion survival fraction was approximately 35%, at 354 MeV it was 50%, and at 489 MeV it was 65%.

An off-line event by event analyzed pion spectrum (after solid angle, energy loss, time of flight, and target beamspot cuts have been applied) is shown in Fig. 1. The energy resolution, as shown in Fig. 1, was typically 200 keV for both data taking runs.

RESULTS

The pion spectrum at $T_p = 354$ MeV and $\theta_{lab} = 21°$ in Fig. 1 is clearly dominated by the 9.50 MeV, $\frac{9}{2}^+$ state, which is predominantly a stretched two-particle–one-hole configuration (2p-1h) with respect to the $^{12}C_{g.s.}$. This selectivity is similar to that previously reported in (p,π^-) reactions[10] and is in contrast to experimental spectra from IUCF (Ref. 11) at $T_p = 200$ MeV and $\theta_{lab} = 30°$, in which the five lowest energy peaks all have approximately the same strength, regardless of the spin of the ^{13}C configuration.

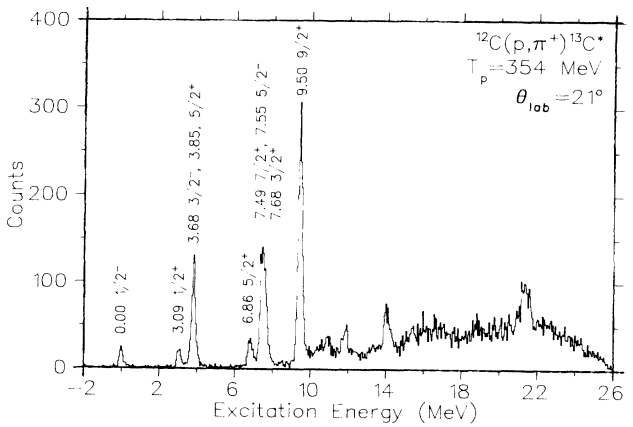

FIG. 1. Pion focal plane spectrum from the second run of the experiment.

TABLE I. List of values for the differential cross sections of the $^{12}C(p,\pi^+)$ reaction leading to various final states of $^{13}C^*$. All quantities shown are in the center of mass frame; angles are in deg and $d\sigma/d\Omega$ are in nb/sr. The numbers in parentheses reflect statistical uncertainties only. The systematic error in the overall normalization has been estimated at 8%, and relative uncertainties have been estimated at 10%.

$\theta_{c.m.}$	$^{13}C_{g.s.}$	$^{13}C^*_{3.09}$	$^{13}C^*_{3.68,\,3.85}$	$^{13}C^*_{6.86}$	$^{13}C^*_{7.49\,7.55\,7.68}$	$^{13}C^*_{9.50}$	$^{13}C^*_{21.4}$
				$T_p=250$ MeV			
31	331(36)	326(36)	1200(71)	464(45)	1120(69)	957(66)	
62	29.1(4.1)	56.7(5.7)	136(9)	123(9)	220(12)	312(15)	
				$T_p=354$ MeV			
22	157(14)	171(15)	944(34)	264(19)	1520(46)	2310(56)	1420(90)
32	106(11)	111(11)	350(20)	123(12)	912(33)	1270(38)	725(55)
37	81.7(9.8)	114(12)	238(17)	107(12)	655(28)	1020(36)	474(29)
48	53.1(5.3)	80.6(6.6)	195(10)	35.6(4.3)	269(12)	322(13)	159(16)
64	15.1(3.2)	21.7(3.7)	73.6(6.9)	24.9(4.0)	115(9)	107(8)	88.1(8.5)
79	5.3(1.4)	2.1(0.9)	13.2(2.3)	2.5(1.0)	39.4(3.8)	32.3(3.6)	
94	8.6(1.6)	6.1(1.3)	14.8(2.1)	1.8(0.7)	12.6(1.9)	27.4(2.8)	
114	3.9(0.8)	<1	1.2(0.4)	<1	8.1(1.1)	5.0(0.9)	
				$T_p=489$ MeV			
21	61.7(8.6)	87.4(10.5)	199(16)	63.2(8.9)	597(27)	786(31)	446(25)
32	28.4(2.6)	54.4(3.6)	114(5)	17.8(2.1)	197(7)	288(8)	72.5(3.9)

The narrowness and the centroid of the 3.68, 3.85 MeV cluster in Fig. 1 indicates that this peak is dominated in strength by the single particle 3.85 MeV state, which has the higher spin. This agrees with the observations of Soga *et al.*[12] at $T_p=156$ MeV, who were able to resolve the states of this cluster. In Fig. 1 the peaks at 11, 12, and 14 MeV previously reported by Dahlgren *et al.*[13] at 185 MeV are also visible. The 21.4 MeV state, which has been recently reported to have an unusual zero analyzing power at 200 MeV,[11] is only clearly visible at forward angles as its cross section falls faster than that of the continuum at larger angles.

Cross sections for all states shown in Fig. 1 are listed in Table I. The systematic error in the overall normalization is estimated at 8%, and an overall relative uncertainty of 10% has been estimated due to the uncertainty in the target angle, integrated beam current, live time, wire chamber efficiency, cut efficiencies, and background subtraction. The uncertainty due to the consistency in the cuts and background subtraction is estimated at less than 8% and was determined by reanalyzing some data with two different sets of cuts.

ENERGY DEPENDENCE OF ANGULAR DISTRIBUTIONS

Figures 2–4 show data from this work, as well as some previously measured angular distributions[12–16] taken at different incident proton energies; these distributions are plotted versus the relativistically invariant Mandelstam variable t, which corresponds to the square of the four-momentum transfer. One must keep in mind that at energies close to pion production threshold, only a small range of four-momentum transfers is accessible, and that this range increases in size, and is restricted to smaller values of t, as the proton energy is increased. Figures for every final state have not been provided as the characteristics of all states can be represented by just a few samples; we shall, however, refer briefly to the characteristics of all these states in the following discussion.

Unlike Soga *et al.*,[12] who multiplied the Uppsala data of Ref. 13 by 1.27 to correct for perceived differences in instrumental normalizations, we have not found it necessary to multiply any data by an arbitrary factor. We have, however, noted that the data of Ref. 13 are reported in the lab frame rather than the center of mass frame,

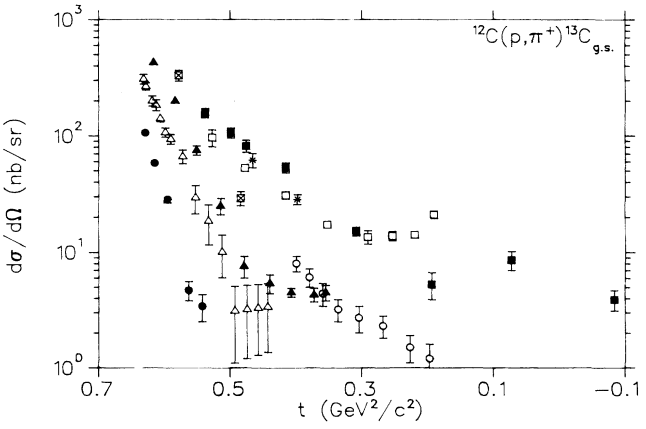

FIG. 2. Angular distributions of the $^{12}C(p,\pi^+)^{13}C_{g.s.}$ reaction plotted vs the square of the four-momentum transfer (t). Plotting symbols indicate the source of data as follows: ● (Ref. 12), 156 MeV; △ (Ref. 13), 185 MeV; ▲ (Ref. 15), 200 MeV; □ (Ref. 16), 250 MeV; ⊠ (this work), 250 MeV; ■ (this work), 354 MeV; ☆ (this work), 489 MeV; ○ (Ref. 14), 800 MeV.

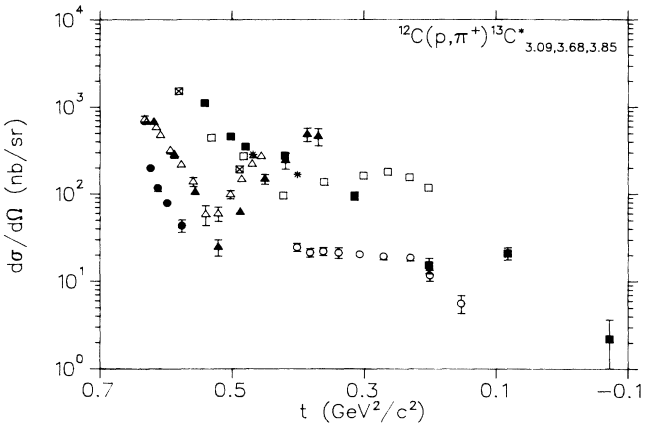

FIG. 3. Angular distributions of the $^{12}C(p,\pi^+)^{13}C^*_{3.09,\,3.68,\,3.85}$ reaction plotted vs the square of the four-momentum transfer (t). This triplet of states is plotted, rather than the $^{13}C^*_{3.09}$ or $^{13}C^*_{3.68,\,3.85}$ states separately, so that the 250 MeV data of Ref. 16 may be used to help show the systematics of the $^{12}C(p,\pi^+)^{13}C^*$ reaction. Plotting symbols indicate the source of data as in Fig. 2.

and have made the appropriate transformation of this data to the center of mass frame. Figures 2–4 do not reveal any gross errors in the normalization of this data; rather, the data of Refs. 13 and 17 agree reasonably well, including statistical errors, at very nearly the same energy.

Note that at 354 MeV the angular distribution of every state falls almost purely exponentially with angle, with no evidence of a backangle peak, even if the state exhibited a very pronounced backangle peak at lower energies. This type of angular distribution, with no dependence on nuclear final state, is presumably due to the very large momentum transfer the (p,π) reaction

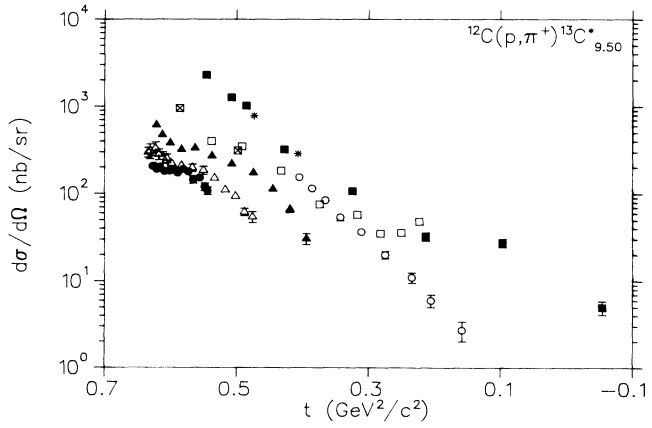

FIG. 4. Angular distributions of the $^{12}C(p,\pi^+)^{13}C^*_{9.50}$ reaction plotted vs the square of the four-momentum transfer (t). Plotting symbols indicate the source of data as in Fig. 2, except ● (Ref. 12), 166 MeV.

accesses at this energy.

A careful analysis of Figs. 2–4 shows that low spin states are comparable in strength to 2p-1h high spin states in only a limited kinematical area of small T_p and forward angle; in other areas 2p-1h high spin states dominate the exclusive pion production cross section. Thus, the stark contrast between the $^{12}C(p,\pi^+)^{13}C^*$ spectra at 200 and 354 MeV, as reported in an earlier section, is characteristic of only a restricted kinematical range. The selectivity of both the (p,π^+) and (p,π^-) reactions for high spin 2p-1h states appear to be very similar, and the empirical explanation for the nonselectivity of (p,π^+) reactions[10] does not appear to hold globally.

Those states which did not display a backangle peak at lower energies, shown in Figs. 2 and 4, have an energy dependence in the range of $0.7 > t > 0.3$ GeV$^2/c^2$ in which the differential cross section is maximum at 354 MeV. Those states which did exhibit a pronounced backangle peak at lower energies, as shown in Fig. 3, also exhibit this energy dependence, but only for momentum transfers below the location of their first minimum ($t \approx 0.5$ GeV$^2/c^2$). This enhancement near the invariant mass of the Δ_{1232} has been previously noted on another target nucleus,[8] and is consistent with a reaction mechanism in which an intermediate Δ_{1232} is produced via the $NN \rightarrow NN\pi^+$ process.

In the region $t < 0.3$ GeV$^2/c^2$, all states have lower differential cross sections at 354 MeV than at 250 MeV; this type of behavior is more difficult to interpret. The $t < 0.5$ GeV$^2/c^2$ energy dependence of those states with low energy backangle peaks (Fig. 3) seems to be nuclear structure related.

In order to more easily observe the energy dependence of the differential cross section, data for the $^{12}C(p,\pi^+)^{13}C_{g.s.}$ and $^{12}C(p,\pi^+)^{13}C^*_{9.50}$ reactions are plotted in Fig. 5 at a constant value of $t = 0.50$ GeV$^2/c^2$. Plotting the differential cross section at a constant four-momentum transfer permits, to a first approximation, the separation of the reaction mechanism from the nuclear structure effects.[8] The use of $\sqrt{s} - m_{^{12}C}$, where s is the relativistic Mandelstam variable corresponding to the square of the center of mass energy, indicates the excitation energy available for one nucleon. Figure 5 indicates an enhancement in the differential cross section which levels off at the invariant mass of the Δ_{1232} ($\sqrt{s} - m_{^{12}C} = 1.232$ GeV).

To relate this enhancement to the role of the Δ_{1232} and the $NN \rightarrow NN\pi^+$ process, the differential cross section of the $pp \rightarrow d\pi^+$ reaction was transformed to the nucleon-nucleus frame using the transformation discussed by Korkmaz *et al.*[11] The result of this transformation, which was to stretch out the high energy tail of an otherwise symmetric peak, is shown at the bottom of Fig. 5; the values plotted are referred to the nucleon-nucleus center of mass frame. Note that the addition of $pp \rightarrow pn\pi^+$ contributions to the $pp \rightarrow d\pi^+$ plot will further enhance the high energy tail and cause it to resemble the nuclear (p,π^+) data even more closely. Therefore, it seems that these excitation functions indicate that the Δ_{1232} does play an important role in (p,π^+) via the $NN \rightarrow NN\pi^+$ reaction mechanism.

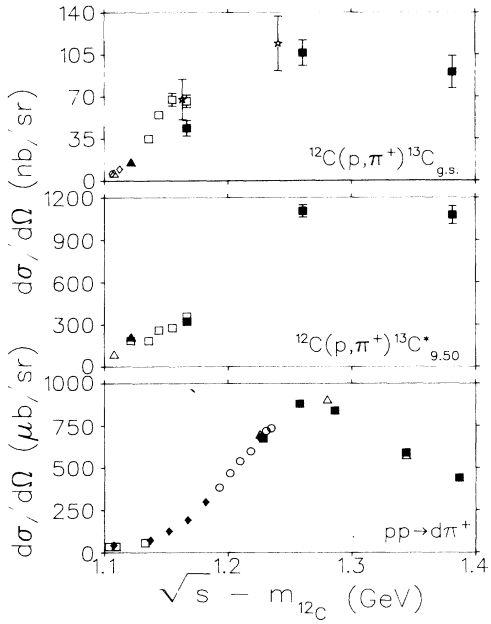

FIG. 5. Differential cross section vs center of mass energy ($\sqrt{s} - m_{^{12}C}$) at a constant square of four-momentum transfer (t) of 0.50 GeV$^2/c^2$ for the $^{12}C(p,\pi^+)^{13}C_{g.s.}$ and $^{12}C(p,\pi^+)^{13}C^*_{9.50}$ reactions. Plotting symbols indicate the source of data as follows: ◇ (Ref. 17), 183 and 190 MeV; △ (Ref. 13), 185 MeV; ▲ (Ref. 15), 200 MeV; □ (Ref. 16), 216, 225, 237, and 250 MeV; ★ (Ref. 6), 246 and 332 MeV; ■ (this work), 250, 354, and 489 MeV. The differential cross sections shown were obtained from the data using either an exponential or Legendre polynomial fit to the distributions. Also shown are differential cross sections for the $pp \rightarrow d\pi^+$ with modifications as explained in the text. Plotting symbols indicate the source of data as follows: ◆ (Ref. 9), ■ (Ref. 18), □ (Ref. 19), △ (Ref. 20), and ○ (Ref. 21). The data from Refs. 18–20 were extracted from Legendre polynomial fits contained in Ref. 22.

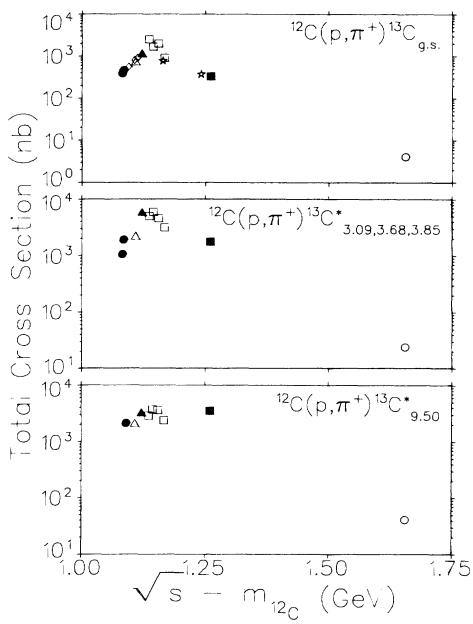

FIG. 6. Energy dependence of the total cross section of the $^{12}C(p,\pi^+)$ reaction leading to three final states of ^{13}C plotted vs the center of mass energy ($\sqrt{s} - m_{^{12}C}$). Plotting symbols indicate the source of data as in Fig. 5 except for the following. $^{12}C(p,\pi^+)^{13}C_{g.s.}$: ● (Ref. 12), 156 and 159 MeV, ◇ (Ref. 17), 170, 183, and 190 MeV; ■ (this work), 354 MeV; ○ (Ref. 14), 800 MeV. $^{12}C(p,\pi^+)^{13}C^*_{3.09,3.68,3.85}$: same as for the ground state, except ● (Ref. 12), 156, 159, and 170 MeV. $^{12}C(p,\pi^+)^{13}C^*_{9.50}$: same as for the ground state, except ● (Ref. 12), 166 MeV.

ENERGY DEPENDENCE OF THE TOTAL CROSS SECTION

Figure 6 shows the energy dependence of the total cross section plotted versus $\sqrt{s} - m_{^{12}C}$. The total cross sections were determined by fitting the angular distributions previously shown with Legendre polynomials, the zeroth order parameter giving the total cross section. The data of Lolos *et al.*[16] have the highest uncertainty in the fit because no measurements were taken at angles smaller than $\theta_{c.m.} = 49°$, where the contribution to the cross section is the largest.

Figure 6 does not show a maximum near the invariant mass of the Δ_{1232}; rather, the maximum cross section occurs about 100 MeV lower than this, corresponding to a beam energy of about $T_p = 225$ MeV. Another interesting feature of Fig. 6 is that the shape of the energy dependence is reasonably independent of final state; this same independence has also been seen for all other nuclear states presented in this paper. Typically, the 354 MeV differential cross section is higher than the 225 MeV differential cross section at the same value of t, but at 354 MeV the (p,π) reaction is restricted to a range of larger momentum transfers. At very high momentum transfers, the exclusive pion production cross section is quite low because of the difficulty of recapturing the extra nucleon in the nucleus. Thus, this 100 MeV shift below the invariant mass of the Δ_{1232} is probably due to an interplay between the increase in cross section due to the Δ_{1232} in the $NN \rightarrow NN\pi^+$ reaction mechanism, and the decrease in differential cross section due to the larger momentum transfers that the reaction is restricted to at higher energies.

COMPARISON OF RESULTS AT 354 MeV WITH THEORETICAL CALCULATIONS

Figure 7 shows the $^{12}C(p,\pi^+)^{13}C_{g.s.}$ data of this work and a relativistic single nucleon reaction mechanism calculation by Cooper and Matsuyama[23] which uses Dirac-Hartree bound states. This calculation does not incorporate the Δ-hole terms that were included in their recent calculation[24] of the $^{16}O(p,\pi^+)^{17}O_{g.s.}$ reaction because of configuration mixing effects for the ^{12}C nucleus; further-

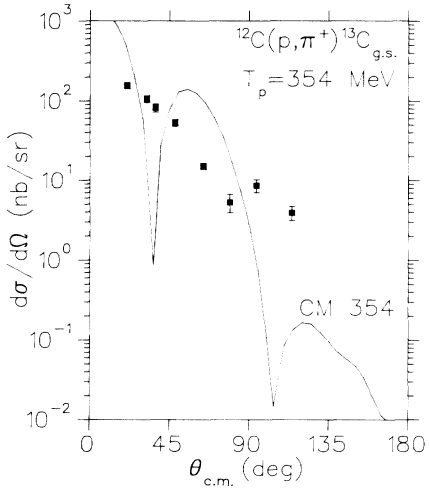

FIG. 7. Relativistic single nucleon model calculation by Cooper and Matsuyama (Ref. 23) shown with data from this work.

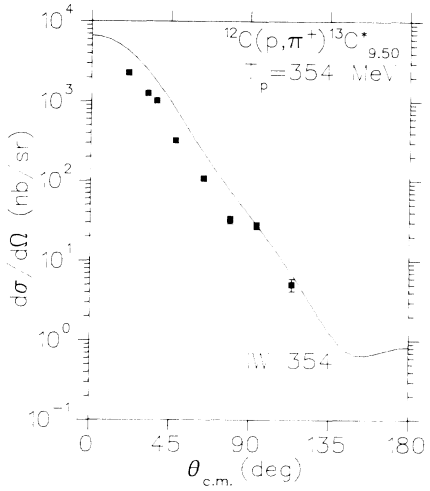

FIG. 8. Two nucleon model calculation by Iqbal and Walker (Ref. 26) shown with data from this work.

more, this calculation incorporates neither proton nor pion distortions. As first discussed by Miller,[25] configuration mixing can be a problem because the single nucleon model (SNM) emphasizes the high momentum components of the nuclear wave functions. Therefore, it is necessary to consider these high momentum components of the final state wave function, even though they have smaller spectroscopic factors than the states of small angular momentum. While the calculation shown oscillates wildly compared to the experimental data, the neglected Δ-hole diagrams will be of comparable magnitude to the calculated single nucleon term and will interfere with this term, smoothing the cross section. Nonetheless, this calculation shows that at least for the $^{12}C(p,\pi^+)^{13}C_{g.s.}$ reaction the single nucleon contribution to the cross section is fairly large.

Figure 8 shows the $^{12}C(p,\pi^+)^{13}C^*_{9.50}$ data of this work and a calculation by Iqbal and Walker[26] which includes diagrams exclusively of the resonant two nucleon model (TNM) type. As can be seen, the agreement between the TNM calculation and the experiment is fairly good. The absolute magnitude of the theoretical prediction is, however, about a factor of 2 too high at forward angles.

Figure 9 shows a similar calculation by Iqbal and Walker at 250 MeV along with previously published data from Ref. 16 as well as this work. The agreement of the TNM calculation with the experimental data is clearly superior at 354 MeV than at 250 MeV. This could indicate that the diagrams which include an intermediate Δ_{1232} resonance are more important to the reaction mechanism at 354 MeV than at 250 MeV; however, any explanation for the discrepancy between the calculation and experiment at 250 MeV must not only take into account neglected nonresonant contributions, but must also include the role of single nucleon diagrams which are not included in this calculation.

Preliminary calculations in progress[27] will hopefully clear up the question of the relative importance of these neglected single nucleon diagrams. Shell model calculations using a Nilsson model with band mixing predict that the $^{13}C^*_{9.50}$ state contains a $^1g_{9/2}$-$^{12}C_{g.s.}$ core configuration with a spectroscopic factor of about 2%. Thus, through this small single particle contribution, it is theoretically possible for the single nucleon model to populate this predominantly 2p-1h state. A plane wave single nucleon model calculation leading to this final state, assuming a spectroscopic factor of 2%, is shown in Fig. 10. Since one expects SNM contributions to play a more important role at lower energies (i.e., lower momentum transfer) than at higher energies, the inclusion of SNM diagrams could bring the calculated differential cross section shown in Fig. 8 closer to the experimental data and thus deemphasize the successful trend observed at 354 MeV.

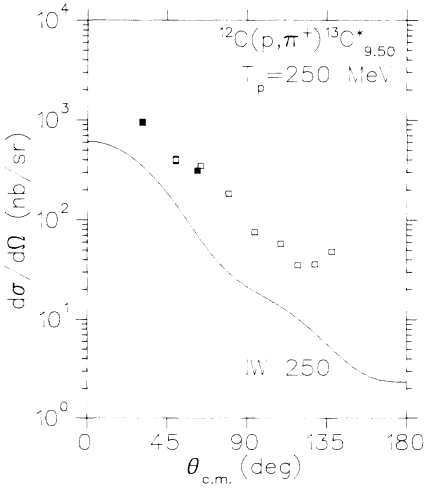

FIG. 9. Two nucleon model calculation by Iqbal and Walker (Ref. 26) shown with data from this work (■) as well as from Ref. 16 (□).

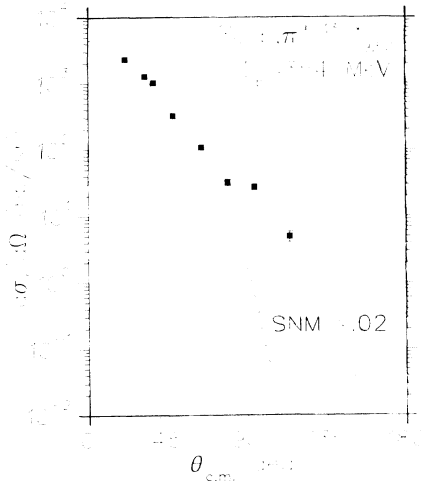

FIG. 10. Relativistic single nucleon model calculation by Cooper and de Takacsy (Ref. 27); this calculation was performed assuming that the spectroscopic factor of the $^{1}g_{9/2}$-$^{12}C_{g.s.}$ component of the $^{13}C^{*}_{9.50}$ state is unity. The calculation is shown with data from this work assuming that the spectroscopic factor of this component is 0.02.

SUMMARY AND CONCLUSIONS

The (p,π^+) reaction mechanism appears to be dominated by two kinematical variables, the total center of mass energy ($\sqrt{s}-m_{^{12}C}$), and the four-momentum transfer (t). The choice of s and t is dictated by the fact that the scattering matrix is only a function of s and t, as far as the kinematic variables are concerned; depending on which variable is being probed, one would get a different picture of the reaction mechanism. In addition, the nuclear form factors for a specific state are dependent on t only.

When $d\sigma/d\Omega$ is plotted at a constant t for different incident energies, the influence of the total energy is isolated. If the Δ_{1232} plays an important role in the (p,π^+) reaction mechanism, the differential cross section should increase with energy up to the invariant mass of the Δ_{1232} and then slowly fall. This type of energy dependence is shown in Figs. 2–4 for at least part of the range of momentum transfer covered by each plot. This is particularly true for those transitions in which the differential cross section falls monotonically with angle. We do not have an explanation for the small t behavior of those states which exhibit a pronounced backangle enhancement at lower energies. Such a dependence on t is probably structure related and one should note that at higher energies these states revert back to the exponential drop characteristic of all the other states.

When one plots the total cross section versus $\sqrt{s}-m_{^{12}C}$, one sees an interplay between a rising cross section due to the Δ_{1232} influence and a declining cross section due to the influence of increasing momentum transfer. Such an interplay would be consistent with Fig. 6, in which the total cross section peaks at an energy about 100 MeV lower than that expected from the Δ_{1232} invariant mass. If this deviation is indeed due to the interplay between these two variables, inclusive (p,π^+) nuclear reactions such as $^{12}C(p,\pi^+)X$, which do not require the extra nucleon to be bound, should show the influence of the $NN\rightarrow NN\pi^+$ channel, while exclusive reactions will show a peak below the invariant mass of the Δ_{1232}.

ACKNOWLEDGMENTS

The authors would like to thank P. Couvert, R. Igarashi, G. Jones, S. I. H. Naqvi, D. F. Ottewell, V. Pafilis, and W. A. Ziegler for their help in the early stages of this experiment, K. P. Jackson and C. A. Miller for their help with the spectrometer, and D. Frekers and D. Sample for their help with the data analysis. We would also like to thank E. D. Cooper and M. J. Iqbal for their valuable comments. This experiment was funded in part by grants from the Natural Sciences and Engineering Research Council of Canada (NSERC).

[1]S. Dahlgren, B. Hoistad, and P. Grafstrom, Phys. Lett. **35B**, 219 (1971).

[2]D. F. Measday and G. A. Miller, Annu. Rev. Nucl. Part. Sci. **29**, 121 (1979).

[3]B. Hoistad, in *Advances in Nuclear Physics*, edited by J. W. Negele and E. Vogt (Plenum, New York, 1979), Vol. 2, p. 135; in *Pion Production and Absorption in Nuclei—1981 (Indiana University)*, edited by Robert D. Bent (AIP, New York, 1982), p. 105.

[4]H. W. Fearing, in *Progress in Particle and Nuclear Physics*, edited by D. Wilkinson (Pergamon, New York, 1981), Vol. 7, p. 113.

[5]P. Couvert, in Proceedings of the Workshop on Studying Nuclei with Medium Energy Protons, Edmonton, 1983, TRIUMF Proceedings Report TRI-83-3, 1983, p. 287.

[6]R. E. Anderson *et al.*, Phys. Rev. C **23**, 2616 (1981).

[7]J. Spuller and D. F. Measday, Phys. Rev. D **12**, 3550 (1975).

[8]P. Couvert and M. Dillig, in Abstracts of the International Conference on High Energy Physics and Nuclear Structure, Versailles (1981), p. 192.

[9]G. L. Giles, Ph.D. thesis, University of British Columbia, 1985; G. L. Giles *et al.* (unpublished).

[10]S. E. Vigdor *et al.*, Nucl. Phys. **A396**, 61c (1983).

[11]E. Korkmaz *et al.*, Phys. Rev. Lett. **58**, 104 (1987).

[12]F. Soga *et al.*, Phys. Rev. C **24**, 570 (1981); F. Soga *et al.*, IUCF Scientific and Technical Report 127, 1980.

[13]S. Dahlgren, P. Grafstrom, B. Hoistad, and A. Asberg, Nucl. Phys. **A211**, 243 (1973).

[14]H. Nann, in *Pion Production and Absorption in Nuclei—1981 (Indiana University)*, Ref. 3, p. 219.

[15]B. Hoistad *et al.*, Phys. Lett. **94B**, 315 (1980); F. Soga *et al.*, IUCF Scientific and Technical Report 127, 1980.
[16]G. J. Lolos *et al.*, Phys. Rev. C **30**, 574 (1984).
[17]M. C. Green, Ph.D. thesis, Indiana University, 1983.
[18]C. Richard-Serre *et al.*, Nucl. Phys. **B20**, 413 (1970).
[19]B. G. Ritchie *et al.*, Phys. Rev. C **24**, 552 (1981).
[20]J. Boswell *et al.*, Phys. Rev. C **25**, 2540 (1982).
[21]J. Hofteizer *et al.*. Nucl. Phys. **A402**, 429 (1983).
[22]G. Jones, in *Pion Production and Absorption in Nuclei—1981 (Indiana University)*, Ref. 3, p. 15.
[23]E. D. Cooper and A. Matsuyama, private communication.
[24]E. D. Cooper and A. Matsuyama, Nucl. Phys. **A460**, 699 (1986).
[25]G. A. Miller, Nucl. Phys. **A224**, 269 (1974).
[26]M. J. Iqbal and G. E. Walker, Phys. Rev. C **32**, 557 (1985); M. J. Iqbal and G. E. Walker, private communication.
[27]E. D. Cooper and N. de Takacsy, private communication.